Correlation of Volume Ratio and Normalized Permittivity in Particle Mixture

Correlation of Volume Ratio and Normalized Permittivity in Particle Mixture

Huarui Wang, Yunjie Yang, (*Member, IEEE)*, Kevin J. Hanley, Jin Y. Ooi, Xipeng Yin and Jiabin Jia, (*Member, IEEE)*

***Abstract*— The volume ratio in the total solid particle mixture is an important parameter indicating the characteristics of particulate mixtures. Therefore, a simple measurement method is desirable. In this paper, the normalized permittivities of two groups of particle mixtures are tested using Electrical Capacitance Tomography (ECT) with the series and parallel models. The experimental results show that normalized permittivity changes obtained from the series ECT model have a very strong linear relationship with the volume ratio of higher permittivity materials in the mixture. The Maxwell Garnett Formula (MGF) can predict the normalized permittivity only after the permittivity of each type of particle is known. The comparison between two methods suggests that ECT with the series model is a better way to monitor the volume ratio in mixtures comprising two different types of solid particle.**

***Index Terms*— Electrical Capacitance Tomography (ECT), Volume ratio, Maxwell Garnett Formula, Normalized permittivity.**

I. Introduction

GRANULAR materials are almost ubiquitous in process industries, for instance, coal powders, biomass particles, and agricultural grains. These materials are usually stored in silos prior to downstream processing. The volume composition ratio of different granular materials in multiphase mixtures is a vital parameter indicating the characteristics of a mixed granular material. Ideally, this information could be retrieved on-line to monitor the status of a granular flow or to apply real-time control to the process. Non-invasive and in-situ methods of measuring solid volume fraction make use of optical techniques [1, 2], CT scanning [3] and the microwave technique [4]. Regarding the optical-based methods, the short penetration depth of the light in systems of denser solids is a major problem. As for CT scanning, in spite of its high spatial resolution, the disadvantages of low temporal resolution, high complexity, high cost and radioactivity restrict its widespread application. The microwave technique uses only two horn-antennas placed opposite each other which results in a low spatial resolution. Electrical Capacitance Tomography (ECT) is one of the industrial process tomography modalities. Its principle is to measure the capacitance between electrode pairs and thereby estimate the permittivity changes inside pipelines or vessels in a visible manner [5]. Due to the advantages of non-invasiveness, non-radiation, high temporal resolution, low cost and ease of use, ECT has been widely applied in monitoring and measuring two-phase flows [6, 7] and particulate processes [8] such as dynamics in a fluidized bed [9] or pneumatic conveying of granular solids [10].

In this paper, we investigate the feasibility of using ECT to measure the volume composition ratio of different solid particles. In particular, the results using two ECT normalization models, the series model and the parallel model, are compared. Then comparisons of the normalized permittivity change from ECT and the Maxwell Garnett Formula (MGF) are carried out based on a series of static experiments.

The paper is organized as follows. In Section II, the principle of ECT and two ECT models are introduced. In Section III, the specifications of the ECT system are presented and the experimental methodology is explained. The experimental results are presented and discussed in Section IV. Finally, conclusions are drawn in Section V.

II. Principle of ECT and Maxwell Garnett Formula

ECT measures the capacitance between all independent combinations of the electrode pairs to reconstruct cross-sectional images with respect to the dielectric permittivity change. The linearized model describing the relationship between capacitance measurement and permittivity change is expressed as

$$\lambda_j = \sum_{k=1}^{M} s_{j,k}\, g_k \quad (j = 1, 2, \cdots, P) \tag{1}$$

where g_k is the normalized permittivity change displayed at the pixel of index k of the reconstructed image; $s_{j,k}$ denotes the normalized sensitivity coefficient at pixel k under the projection-measurement j; P denotes the total number of measurements (P = 28 in this work); M is the total number of pixels in the image (M = 3228 in this work); λ_j denotes the normalized capacitance change at projection-measurement j.

This research is supported by the CareerWISE Placement of EQUATE Scotland and National Natural Science Foundation of China (NSFC 51206070), Jiangsu Provincial Natural Science Foundation of China (BK20131128).

Y. Yang, K. J. Hanley, J. Y. Ooi, X. Yin and J. Jia are with the School of Engineering, University of Edinburgh, Edinburgh, UK (correspondence e-mail: jiabin.jia@ed.ac.uk).

H. Wang is working in the Jiangsu Key Laboratory of Advanced Laser Materials and Devices, School of Physics and Electronics Engineering, Jiangsu Normal University, Xuzhou, China.

To date, most ECT systems are calibrated in advance using a lower permittivity material and a higher permittivity material; then the distribution of high-permittivity material in the background of low-permittivity material can be imaged. Using normalized capacitance data rather than the absolute value is a common means of image reconstruction. The conventional normalization approach assumes that the distribution of the two materials is in parallel and the normalized capacitance is the following linear function with respect to the measured capacitance:

$$\lambda_j = \frac{C_j - C_{j,low}}{C_{j,high} - C_{j,low}} \tag{2}$$

where $c_{j,low}$ and $c_{j,high}$ are the measured capacitance when the sensor is filled with the low- and high-permittivity materials under the projection-measurement *j*, respectively, and c_j is the measured capacitance of the mixture of two materials. However, this approach is more suitable for a stratified distribution with the interface in between a pair of horizontally separated electrodes [11]. When two materials are mixed more uniformly, using the series model [11] is a more suitable approach, the normalized capacitance change λ_j at projection-measurement *j* is expressed as

$$\lambda_j = \frac{1/C_j - 1/C_{j,low}}{1/C_{j,high} - 1/C_{j,low}} \tag{3}$$

Once the normalised capacitance λ_j is derived, the process of image reconstruction is to estimate g_k (k=1, 2, ⋯, M) at all pixels based on the normalized sensitivity coefficient $s_{j,k}$, which is a typical inverse problem. In this paper, the inverse problem is solved by the Linear Back Projection (LBP) algorithm [12] given by

$$g_k = \sum_{k=1}^{M} s_{j,k}^T \lambda_j \left(j = 1, 2, \cdots, P \right) \tag{4}$$

Averaging g_k at all the pixels gives the overall normalized permittivity change *g* based on ECT. Alternatively, the normalized permittivity change *g* can be directly calculated as

$$g = \frac{\varepsilon - \varepsilon_{low}}{\varepsilon_{high} - \varepsilon_{low}} \tag{5}$$

where ε_{low} and ε_{high} are the low and high permittivities of the two reference materials comprising the mixture. ε is the effective permittivity of the mixture.

The effective permittivity of composites containing two or more phases is determined not only by the volume fraction but also the dielectric permittivity of each phase. The effective permittivity can be predicted by a conventional model, i.e., the Maxwell Garnett formula (MGF) [13]. A general explicit MGF is used to estimate the effective dielectric permittivity ε_{eff} of the mixture. This is expressed as

$$\varepsilon_{eff} = \varepsilon_{air} + 3\varepsilon_{air} \frac{\sum_{i=1}^{n} f_i \frac{\varepsilon_i - \varepsilon_{air}}{\varepsilon_i + 2\varepsilon_{air}}}{1 - \sum_{i=1}^{n} f_i \frac{\varepsilon_i - \varepsilon_{air}}{\varepsilon_i + 2\varepsilon_{air}}} \tag{6}$$

where ε_i is the dielectric permittivity of the i^{th} type of phase (solid particles in this work) in a host phase (air in this work). ε_{air} denotes the relative permittivity of air; f_i is the volume fraction of the i^{th} type of phase; *n* is the number of different phases.

To obtain ε_{eff} using Eq. (6), the individual value of ε_i has to be known. In contrast, it is unnecessary for ECT to know the exact values of ε_{low} and ε_{high} before the normalized permittivity change *g* is obtained, which is one of the advantages of the ECT.

III. Experiment Setup and Methodology

A. ECT System

Fig. 1 shows a picture of the ECT system and the sensor used in this study. The ECT system utilized in the experiments is based on a novel digital architecture [14]. It supports up to 32 electrodes and each electrode can be configured individually through a customized user interface. Hence the system not only deploys the traditional ECT sensing strategy but also enables flexible projection-measurement combinations. Two groups of capacitance measurement planes are integrated into the system and it is capable of achieving simultaneous measurement of a twin-plane sensor with up to 16 electrodes on each plane. The frame rate of the system can reach up to 1562 frames per second.

The quality of capacitance measurement directly determines the reliability of subsequent data analysis. The signal to noise ratio (SNR) is calculated to evaluate the precision of the ECT system, which is defined as

$$SNR = 10\log \frac{\sum_{l=1}^{L} \left[C(l) \right]^2}{\sum_{l=1}^{L} \left[C(l) - \bar{C} \right]^2} \tag{7}$$

where *C* is the measured capacitance vector with respect to time; $\bar{C}$ is the mean of each element of the vector; *L* is the total image frame number. When the ECT sensor was empty, 5000 frame measurements were taken continuously at a frame rate of 714 frames per second. The SNR profile of all electrode pairs was calculated according to Eq. (7) and the result is shown in Fig. 2. The SNR of adjacent electrode pairs is above 76 dB and the SNR of non-adjacent electrode pairs is above 62.5 dB. When the sensor is empty, the measured capacitance values are shown in Fig. 3. The capacitance between adjacent electrodes is above 0.8 pF and the capacitance between other electrodes is below 0.2 pF. The result indicates that the measurement is stable enough for further data acquisition and analysis. Other parameters of the ECT system used in this work such as frame rate, excitation voltage and frequency are presented in Table I.

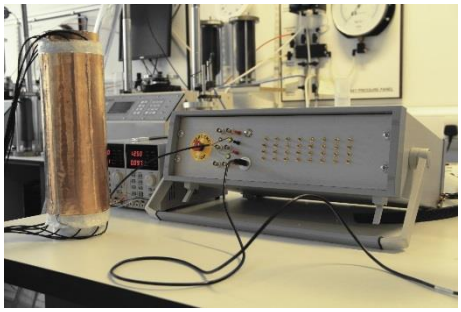

Fig. 1. Picture of the ECT system and the sensor.

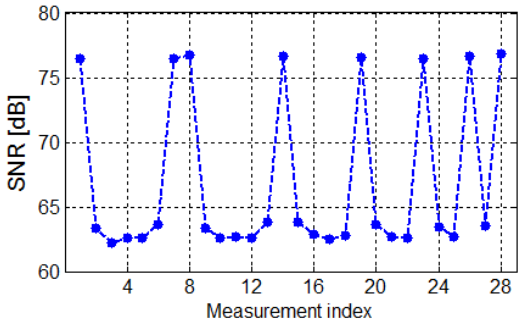

Fig. 2. SNR of the ECT system on the empty sensor.

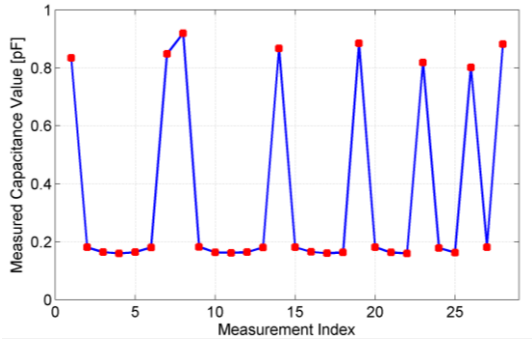

Fig. 3. Measured capacitance values on the empty sensor.

Table I. Specifications of the ECT system.

Configuration	Sensing plane 1	Sensing plane 2
Electrode number	8	8
Frame rate	714 fps	714 fps
Excitation voltage	14 V_{pp}	14 V_{pp}
Excitation frequency	200 kHz	200 kHz
Maximum SNR	76.73 dB	75.67 dB
Minimum SNR	62.25 dB	63.21 dB

B. *Experiment Setup*

A flat bottom silo of 100 mm diameter and 370 mm axial length was used in these experiments, as illustrated in Fig. 4(b). A schematic of the ECT sensor attached to the external wall of the silo is shown in Fig. 4(a). The central distance between the two sensing planes of the ECT sensor is 150 mm. Each plane has 8 copper electrodes, each of which is 36 mm in width and 100 mm in length. The axial earth ground electrodes between the two planes are included to reduce fringe effects [15]. The ECT system has a variable frame rate. For all experiments in this paper, the frame rate was set at 714 frames per second per

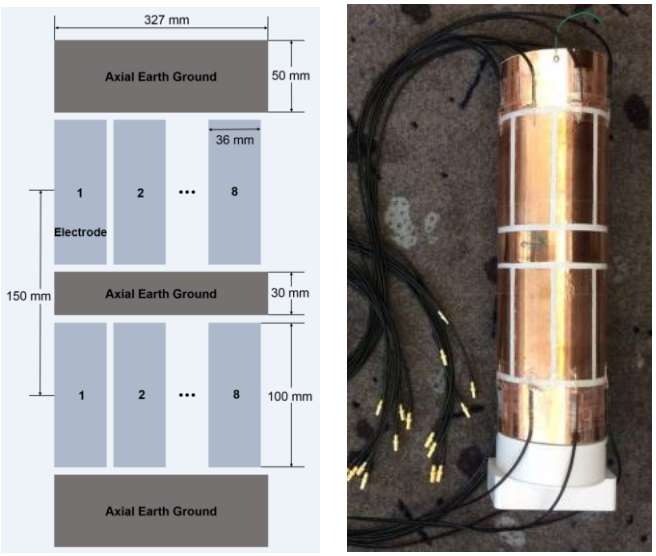

(a) (b)

Fig. 4. Experiment setup. (a) Schematic of the ECT sensor. (b) Silo with ECT sensor.

plane. Only one sensing plane is sufficient for measuring the capacitance change for the derivation of permittivity change. However, using both planes enables more data to be captured to analyze the measurement certainty.

C. *Experiment Methodology*

The purpose of this work is to verify the accuracy of utilizing ECT to measure the volume composition ratio of different solid particles in the gas-solid$_1$-solid$_2$ three-phase composite mixture. According to the geometry of the ECT sensor, a normalized sensitivity coefficient $s_{j,k}$ in Eq. (1) was calculated in advance using the finite-element-method-based software COMSOL Multiphysics. The ECT sensor was firstly filled with a low-permittivity material to obtain the low capacitance measurement for use in Eq. (2) and (3). Similarly, a high-capacitance material was used to obtain c_{high}. Then the ECT sensor was filled with mixtures of the two particulate materials at different volume ratios to create any capacitance measurement c between the two reference capacitances. The normalized capacitance change λ was computed according to Eq. (2) and (3). Finally, the normalized permittivity change was calculated inversely based on Eq. (4) to find the volume composition ratio. The normalized permittivity change can also be derived after each term in Eq. (5) was obtained by repeatedly using the MGF depicted in Eq. (6). Therefore, to use the MGF, the dielectric permittivity of each type of particles must be known. However, it is difficult to get these values in practice. The true solid volume fraction could be calculated after the volume, mass and density of solid particles were measured. The true volume fractions could be used to validate the relation between normalized permittivity and volume fraction. The experimental methodology is illustrated in the flow chart in Fig. 5.

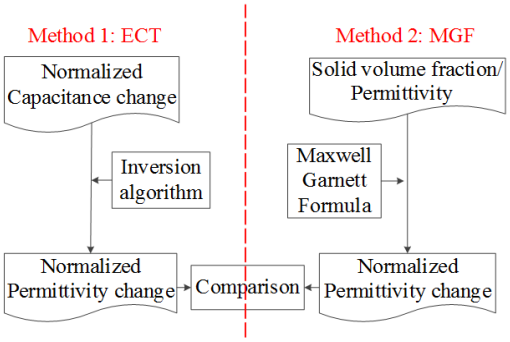

Fig. 5. Flowchart of experiment and analysis procedure.

The left-hand side of Fig. 5 indicates that the normalized permittivity change g is reconstructed from normalized capacitance measured by the ECT system. The right-hand side of Fig. 5 demonstrates that the solid volume fraction and dielectric permittivity are substituted into the MGF to obtain the normalized permittivity change. Finally, the normalized permittivity changes obtained from these two methods are compared.

IV. Experiment Results and Discussion

A. Multiphase Particulate Mixture: Polyethylene Pellets, Rice Grains and Air

A multiphase mixture is created when particles of differing permittivity are mixed together. In this subsection, slender ellipsoidal rice grains and polyethylene pellets are used. The mixture samples with different composition fraction in the ECT sensor are illustrated in Fig. 6. The ECT sensor filled with rice grains was regarded as the high reference point c_{high} in Eq. (3), and the ECT sensor filled with polyethylene pellets was regarded as the low reference point c_{low}. In the multiphase system, much attention needs to be paid to the effect of different volume composition ratio of the two types of particles on normalized permittivity change. The volume ratio of rice grains to total solid particle composition is defined as

$$\frac{V_{rice}}{V_{total}} = \frac{V_{rice}}{V_{poly} + V_{rice}} = \frac{M_{rice}/\rho_{rice}}{M_{poly}/\rho_{poly} + M_{rice}/\rho_{rice}} \quad (8)$$

where V_{poly} and V_{rice} denote the volumes of polyethylene pellets and rice grains, respectively, and V_{total} is the total volume of solid particles. Each constituent volume can be calculated from its mass and intrinsic density. The intrinsic densities for rice grains and polyethylene pellets are 1468.8 kg/m^3 and 911.4 kg/m^3 in these experiments.

Fig. 7 shows the reconstructed images of different volume ratio of rice grains to total solid composition from 0.10 to 0.89. The mass of each type of solid particle is shown in Table II. In addition to the general trend of increasing normalized permittivity change with the increase of the volume ratio, the random heterogeneous distribution of rice grains can also be observed.

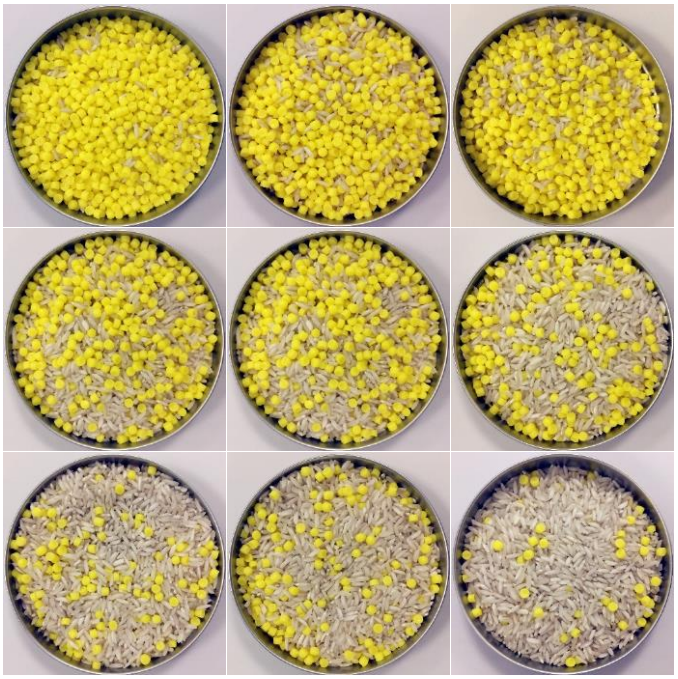

Fig. 6. Mixture samples of rice grains (white) and polyethylene pellets (yellow) in the ECT sensor. From left to right and top to bottom, the volume ratio of rice grains to total solid composition is 0.10, 0.19, 0.29, 0.38, 0.48, 0.58, 0.68, 0.79 and 0.89.

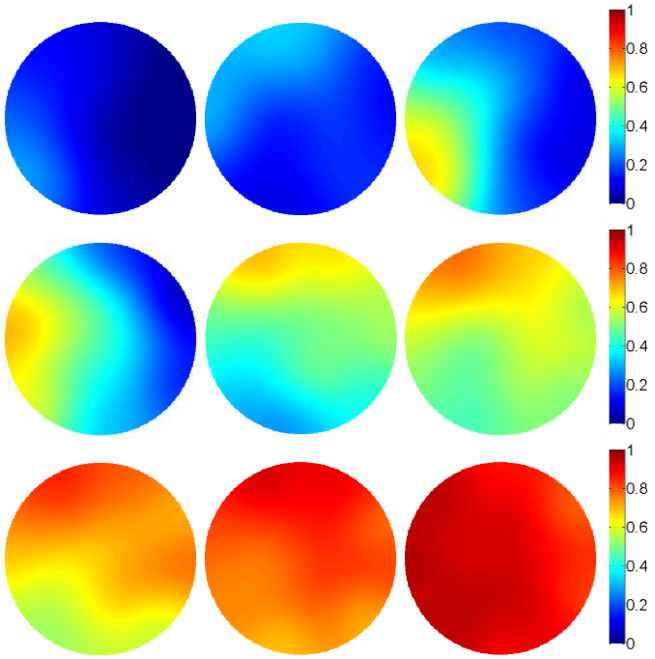

Fig. 7. Reconstructed ECT images corresponding to Fig. 6.

Fig. 8 shows the dependence of the normalized permittivity change from ECT on the volume ratio of rice grains to total solid volume. Both the results using the series model depicted in Eq. (3) and the parallel model depicted in Eq. (2) are presented. The true volume ratios of rice grains are computed using Eq. (8). The absolute errors between the results based on the series model and the true values are presented in Table III. There is a strong linear relationship between the normalized permittivity based on the series ECT model and the true volume

ratio. In contrast, the normalized permittivity derived from the parallel ECT model is always underestimated, except at the volume ratios of 0 and 1. Therefore, results based on the series model outperform those based on the parallel model. This is due to the ability of the series model to eliminate part of the nonlinear effect in the mapping from permittivity distribution to capacitance.

Table II. True volume ratio of rice grains and mass of each type of particle in Fig. 7.

True volume ratio	**0.00**	**0.10**	**0.19**	**0.29**	**0.38**	**0.48**
Mass of rice grains [kg]	0	0.254	0.498	0.742	0.986	1.230
Mass of polyethylene pellets [kg]	1.640	1.476	1.312	1.148	0.984	0.820
True volume ratio	**0.58**	**0.68**	**0.79**	**0.89**	**1.00**	
Mass of rice grains [kg]	1.474	1.718	1.962	2.206	2.450	
Mass of polyethylene pellets [kg]	0.656	0.492	0.328	0.164	0	

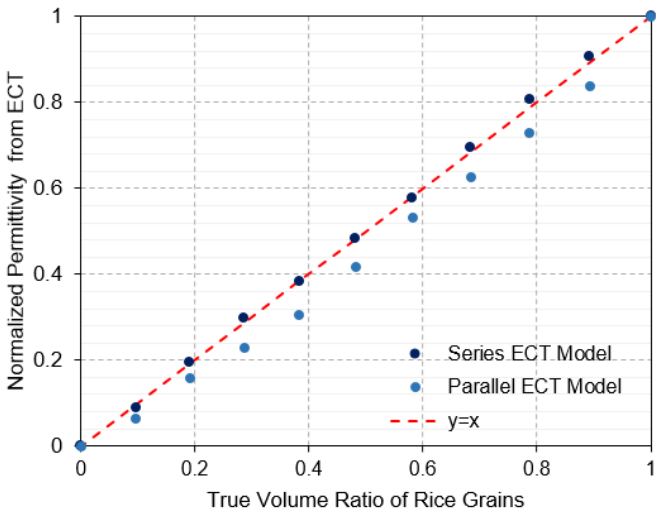

Fig. 8. Dependence of normalized permittivity from ECT on the true volume ratio of rice grains to total solid.

Table III. Absolute errors between normalized permittivity obtained from the series ECT model and true volume ratio in Fig. 8.

True volume ratio	**0.00**	**0.10**	**0.19**	**0.29**	**0.38**	**0.48**
Absolute Error [%]	0.00	0.72	0.33	1.28	0.12	0.14
True volume ratio	**0.58**	**0.68**	**0.79**	**0.89**	**1.00**	
Absolute Error [%]	0.35	1.03	1.86	1.42	0.00	

According to the result indicated in Fig. 8 and Table II, the volume composition ratio of rice grains to the total solid volume could be predicted using the normalized permittivity change from ECT with high accuracy. In order to demonstrate the reliability of the ECT measurement, the volumes of polyethylene pellets and rice grains are used as known data to calculate normalized permittivity change in the following steps. In the multiphase mixture, Eq. (5) is rewritten as

$$g=\frac{\varepsilon_{eff}-\varepsilon_{eff1}}{\varepsilon_{eff2}-\varepsilon_{eff1}} \tag{9}$$

where ε_{eff} is the effective permittivity when the ECT sensor is filled with the mixture of polyethylene pellets and rice grains. ε_{eff} is calculated from the three-phase explicit MGF in Eq. (6); f_i is their volume fraction in the silo ($i=1$ for polyethylene pellets, $i=2$ for rice grains).

$\varepsilon_{eff\,1}$ and $\varepsilon_{eff\,2}$ are the effective permittivities when the ECT sensor is filled only with the low- and high-permittivity particles separately (polyethylene pellets and rice grains, respectively). These two cases belong to a two-phase system. Therefore, the two-phase MGF is used to calculate the two effective permittivities, which are expressed as

$$\begin{cases} \varepsilon_{eff\,1}=\varepsilon_{air}+3\varepsilon_{air}\dfrac{f_{full1}\dfrac{\varepsilon_1-\varepsilon_{air}}{\varepsilon_1+2\varepsilon_{air}}}{1-f_{full1}\dfrac{\varepsilon_1-\varepsilon_{air}}{\varepsilon_1+2\varepsilon_{air}}} \\ \varepsilon_{eff\,2}=\varepsilon_{air}+3\varepsilon_{air}\dfrac{f_{full2}\dfrac{\varepsilon_2-\varepsilon_{air}}{\varepsilon_2+2\varepsilon_{air}}}{1-f_{full2}\dfrac{\varepsilon_2-\varepsilon_{air}}{\varepsilon_2+2\varepsilon_{air}}} \end{cases} \tag{10}$$

where f_{full1} and f_{full2} are the volume fractions when the ECT sensor is filled only with polyethylene pellets or rice grains. f_{full1} and f_{full2} are found as 0.62 and 0.57 based on the weight of the solid in the silo, intrinsic density, diameter of the silo and the fill height.

Substituting Eq. (10) and Eq. (6) into Eq. (9) yields the normalized permittivity change. During the calculation, the relative permittivity of air equals to 1 and the relative permittivity of rice grains ε_1 and polyethylene pellets ε_2 are estimated to be 4 and 2.26, respectively.

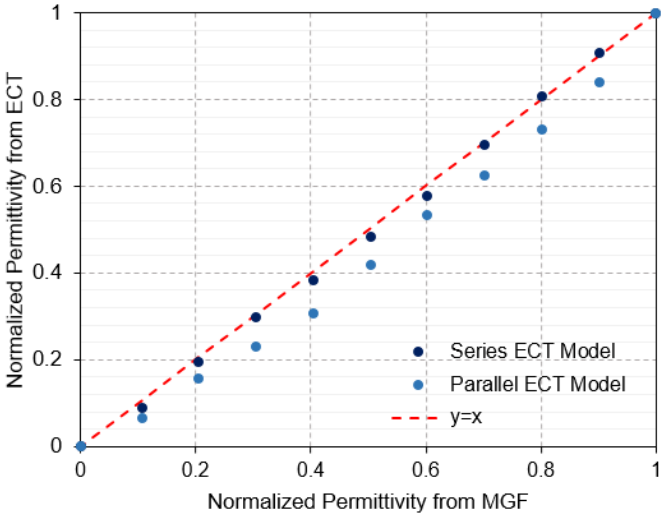

Fig. 9. Correlation of normalized permittivity from two ECT models and MGF.

The relationships between the normalized permittivity changes from both ECT models and that from the MGF are plotted in Fig. 9. The absolute errors between the ECT result based on the series model and MGF are listed in Table IV. A near-perfect linear correlation exists, and the maximum absolute error is 2.42%. ECT can reconstruct normalized permittivity change without knowing the permittivity of particles, while the method based on MGF needs more prior knowledge regarding the permittivity of rice grains and polyethylene pellets.

Table IV. Absolute errors between ECT and MGF calculation in Fig. 9.

True volume ratio	**0.00**	**0.10**	**0.19**	**0.29**	**0.38**	**0.48**
Absolute Error [%]	0.00	1.74	1.21	0.62	2.23	2.03
True volume ratio	**0.58**	**0.68**	**0.79**	**0.89**	**1.00**	
Absolute Error [%]	2.42	0.77	0.49	0.65	0.00	

B. Multiphase Particulate Mixture: Polyethylene Pellets, Mung Beans and Air

In this subsection, slender ellipsoidal rice grains are replaced by the approximately spherical mung beans as shown in Fig. 10. The mass of each type of particle is given in Table V. The volume ratio of mung beans is determined by Eq. (8) in which the subscript 'rice' is replaced by 'mung bean'. The intrinsic density for mung beans and polyethylene pellets are 1314.9 kg/m^3 and 911.4 kg/m^3, respectively. The reconstructed ECT images in Fig. 11 correspond to the mixture sample in Fig. 10. Again, the trend of permittivity change is evident in the reconstructed images, despite some noticeably heterogeneous distributions appearing when the volume ratio of mung beans is in the range of 0.30–0.80.

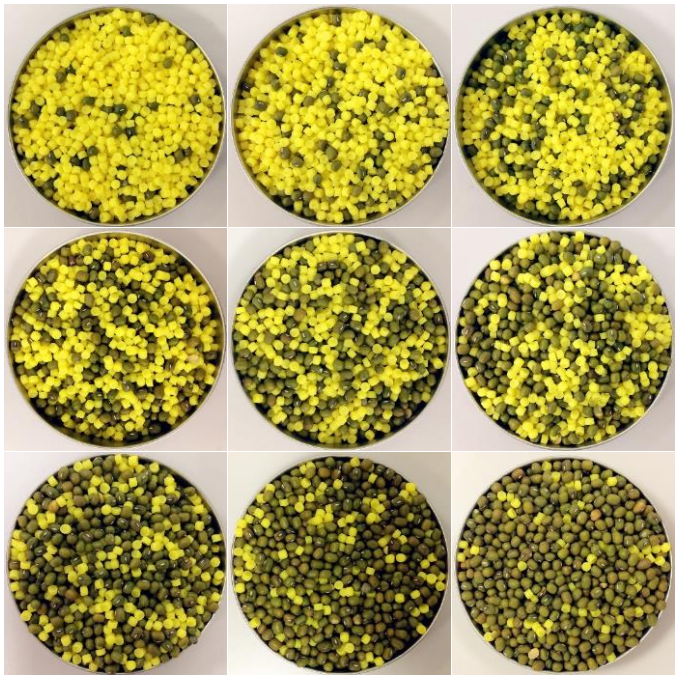

Fig. 10. Mixture samples of mung beans (green), polyethylene pellets (yellow) in the ECT sensor. From left to right and top to bottom, the volume ratio of mung beans to total solid is 0.10, 0.20, 0.30, 0.40, 0.50, 0.59, 0.69, 0.79 and 0.89.

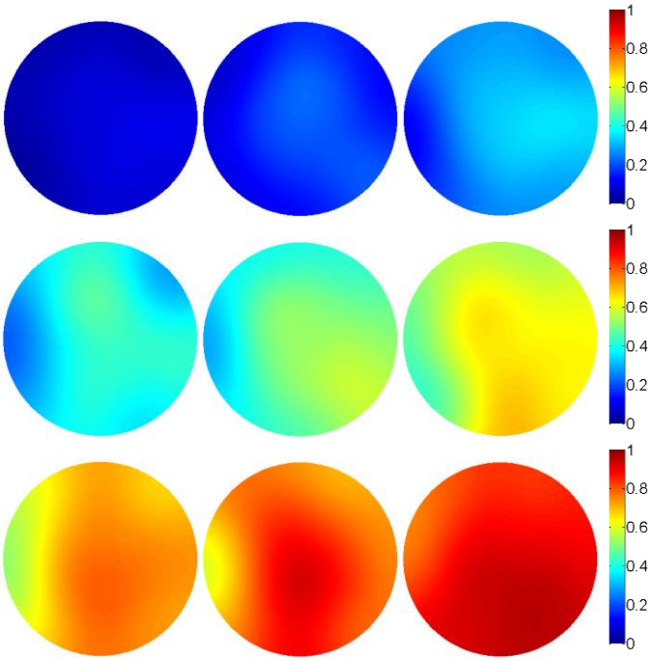

Fig.11. Reconstructed ECT images corresponding to Fig. 10.

Table V. True volume ratio of mung beads and mass of each type of particle in Fig. 10.

True volume ratio	**0.00**	**0.10**	**0.20**	**0.30**	**0.40**	**0.50**
Mass of mung beans [kg]	0.00	0.242	0.484	0.726	0.968	1.210
Mass of polyethylene pellets [kg]	1.670	1.506	1.342	1.178	1.014	0.850
True volume ratio	**0.59**	**0.69**	**0.79**	**0.89**	**1.00**	
Mass of mung beans [kg]	1.452	1.694	1.936	2.178	2.530	
Mass of polyethylene pellets [kg]	0.686	0.522	0.358	0.194	0	

Fig. 12 shows the strong linear relation between the normalized permittivity change from ECT based on the series model and the true volume ratio of mung beans to the total solid volume. This suggests the volume ratio of mung beans could be predicted from the normalized permittivity change calculated by ECT. The absolute errors between the ECT result based on the series model and MGF are presented in Table VI. It indicates that a very strong linear correlation exists, as was the case for the mixture of rice and polyethylene pellets. In this case, the maximum absolute error is 3.63%.

In order to demonstrate the reliability of the ECT measurement result, the volumes of polyethylene pellets and mung beans are used as known data to calculate normalized permittivity change in the same manner as in subsection A. During the calculation of MGF, the relative permittivity of air equals to 1 and the relative permittivities of mung beans and

polyethylene pellets are estimated to be 10 and 2.26, respectively. f_{full1} and f_{full2} are 0.63 and 0.66 in this case.

The results are shown in Fig. 13 which plots the relationship between the normalized permittivity changes from ECT using both the series and parallel models and that from the MGF. Again, a stronger linear relationship exists between the result based on the series model and the MGF-based result. The slope of the line is positive, so there is a positive correlation between the normalized permittivity changes from the two different methods. The straight line almost passes through the origin of the coordinate plane. This demonstrates that the normalized permittivity values obtained from series-model ECT have very good agreement with those from MGF. The parallel ECT model non-linearly underestimates the normalized permittivity, except at the volume ratios of 0 and 1. Table VII shows the absolute error of calculations by the ECT method using the series model and MGF method. The maximum error is 4.38%, confirming that the differences between the results using ECT and MGF methods are small.

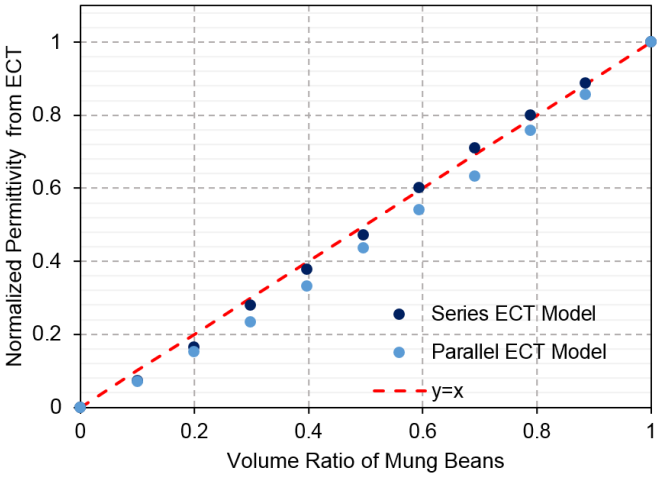

Fig. 12. Dependence of normalized permittivity from ECT on the true volume ratio of mung beans to total solid.

Table VI. Absolute error of normalized permittivity obtained from the series ECT model and true volume ratio in Fig. 12.

True volume ratio	**0.00**	**0.10**	**0.20**	**0.30**	**0.40**	**0.50**
Absolute Error [%]	0.00	2.72	3.63	2.06	2.01	2.59
True volume ratio	**0.59**	**0.69**	**0.79**	**0.89**	**1.00**	
Absolute Error [%]	0.68	1.83	1.02	0.05	0.00	

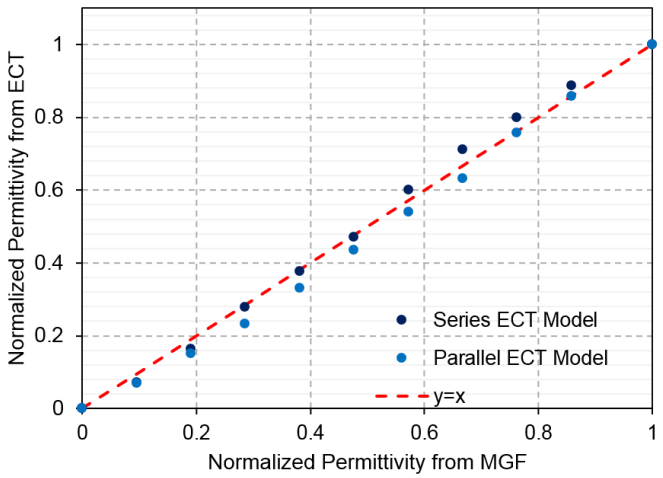

Fig. 13. Correlation of normalized permittivity from two ECT models and MGF.

Table VII. Absolute errors of ECT and MGF calculation in Fig. 13.

True volume ratio	**0.00**	**0.10**	**0.20**	**0.30**	**0.40**	**0.50**
Absolute Error [%]	0.00	2.23	2.69	0.71	0.29	0.56
True volume ratio	**0.59**	**0.69**	**0.79**	**0.89**	**1.00**	
Absolute Error [%]	2.99	4.38	3.75	2.93	0.00	

V. Conclusions

In this paper, the volume composition ratio of different particles in a three-phase mixture is investigated using the parallel and series Electrical Capacitance Tomography (ECT) model and the Maxwell Garnett Formula (MGF). The true volume ratios of high-permittivity material in the total solid are measured in the range of 0 to 1 to correlate with the normalized permittivity. The experimental results prove the volume ratio of high-permittivity material has a strong linear relationship with the normalized permittivity, which can be obtained from both ECT and MGF. When ECT is applied, the series model outperforms the parallel model in terms of accuracy. To use MGF, the permittivity of each type of material must be known; however, that is not the case for ECT.

This work demonstrates that ECT is able to detect the volume composition ratio of mixtures containing two different types of solid particles. A potential application of the proposed method could be on-line monitoring for solid particle processing in the food, pharmaceutical and biomass industries. In pneumatic conveying systems, the solid particles have a lower volume fraction than the static solid particles in the silo. Future work will study how the techniques discussed in this paper could be applied in practical pneumatic conveying loops.

References

[1] R. Iyer, S. Hegde, D. Singhal and W. Malick, “A novel approach to determine solid fraction using a laser-based direct volume measurement

device", *Pharmaceutical Development and Technology*. vol.19(5), pp. 577-582, 2014.

[2] S. Steinbach and L. Ratke, "In situ optical determination of fraction solid", *Scripta Materialia*, vol. 50(8), pp.1135–1138, 2004

[3] J. Borges, L. Pires and A. Pereira, "Computed Tomography to Estimate the Representative Elementary Area for Soil Porosity Measurements", *The Scientific World Journal*, 2012.

[4] C. Baer, T. Musc, M. Gerding, and M. Vogt, "Evaluation of a concept for density measurement of solid particle flows in pneumatic conveying systems with microwaves (8–12 GHz)", *Advances in Radio Science*, vol. 9, pp. 27-30, 2011.

[5] W. Yang, "Design of electrical capacitance tomography sensors", *Measurement Science and Technology*, vol. 21(4), pp. 042001, 2010.

[6] M. V. Sardeshpande, S. Harinarayan, and V. V. Ranade, "Void fraction measurement using electrical capacitance tomography and high speed photography", *Chemical Engineering Research and Design*, vol. 94, pp. 1-11, 2015.

[7] R. Banasiak, R. Wajman, T. Jaworski, P. Fiderek, H. Fidos, J. Nowakowski, and D. Sankowski, "Study on two-phase flow regime visualization and identification using 3D electrical capacitance tomography and fuzzy-logic classification", *International Journal of Multiphase Flow*, vol. 58, pp. 1-14, 2014.

[8] W. Zhang, C. Wang, W. Yang and C. Wang, "Application of electrical capacitance tomography in particulate process measurement – A review", *Advanced Power Technology*, vol. 25, pp. 174-188, 2014.

[9] H. Wang and W. Yang, "Scale-up of an electrical capacitance tomography sensor for imaging pharmaceutical fluidized beds and validation by computational fluid dynamics", *Measurement Science and Technology*, vol. 22 (10), pp. 104015, 2011.

[10] K. Zhu, S. M. Rao, C. Wang, S. Sundaresan, "Electrical capacitance tomography measurements on vertical and inclined pneumatic conveying of granular solids", *Chemical Engineering Science*, vol. 58, pp. 4225-4245, 2003.

[11] W. Yang "An improved normalisation approach for electrical capacitance tomography", *1st World Congress on Industrial Process Tomography, Great Manchester*, April 14-17, 1999.

[12] Y. Li, W. Yang, C. G. Xie, S. Huang, Z. Wu, D. Tsamakis, and C. Lenn, "Gas/oil/water flow measurement by electrical capacitance tomography", *Measurement science and technology*, vol. 24, no. 7, 074001, 2013.

[13] F. Frisone, *Theory and Phenomena of Metamaterials*. Taylor and Francis Group, LLC, 2009.

[14] Y. Yang, L. Peng, and J. Jia, "A novel multi-electrode sensing strategy for electrical capacitance tomography with ultra-low dynamic range." *Flow Measurement and Instrumentation*, vol. 53, Part A, pp. 67–79, 2017.

[15] J. Sun and W. Yang, "Fringe effect of electrical capacitance and resistance tomography sensors", *Measurement and Science and Technology*, vol. 24, pp. 1-15, 2013.